ACS Catalysis

RESEARCH ARTICLE

pubs.acs.org/acscatalysis

Shape Selectivity in the Conversion of Methanol to Hydrocarbons: The Catalytic Performance of One-Dimensional 10-Ring Zeolites: ZSM-22, ZSM-23, ZSM-48, and EU-1

Shewangizaw Teketel,[†] Wegard Skistad,[†] Sandrine Benard,[†] Unni Olsbye,[†] Karl Petter Lillerud,[†] Pablo Beato,[‡] and Stian Svelle*[,†]

[†]inGAP Center for Research Based Innovation, Department of Chemistry, University of Oslo, P.O. Box 1033 Blindern, N-0315 Oslo, Norway

[‡]Haldor Topsøe, Nymøllevej 55, DK-2800 Kgs. Lyngby, Denmark

Supporting Information

ABSTRACT: The methanol-to-hydrocarbon (MTH) reaction, a process in which low-value carbon-rich feedstocks are converted to value-added petrochemical products, is studied over one-dimensional 10-ring zeolites: ZSM-22 (TON), ZSM-23 (MTT), ZSM-48 (*MRE), and EU-1 (EUO). The latter three are little studied as MTH catalysts and were expected to display interesting product-shape-selective properties. The influence of slight differences in channel systems of the materials (size and shape) on product distribution and stability is investigated under various reaction conditions. In addition, the influence of coke deposition on product selectivity is investigated. Temperatures between 350 and 500 °C and WHSV between 2 and 6 g g^{-1} h^{-1} are investigated using a fixed bed reactor. The products are analyzed using online GC, and hydrocarbons trapped in the channels of the material during the reaction were liberated using the standard HF dissolution procedure and analyzed using GC/MS. Despite the small differences in the channel shape and dimension, the materials displayed very different product spectra. The catalysts converted comparable amounts of methanol before complete deactivation at their optimum MTH condition. Except for EU-1, all the catalysts gave high selectivity for hydrocarbons in the boiling range of gasoline fuel, C_{5+} fraction. Unlike ZSM-22 and ZSM-23, the EU-1 and ZSM-48 catalysts displayed notable amounts of aromatics in their C_{5+} fraction. Such compounds are good octane boosters. However, because of environmental problems, there are limits on aromatics in gasoline. For ZSM-22, ZSM-23, and EU-1 catalysts, the deposition of coke within the channels does not affect the selectivity. Rather, the change in selectivity with reaction time can be regarded as a change in contact time. The involvement of the 12-ring side pocket of EU-1 zeolites for the MTH reaction is indicated both by the unexpected catalytic behavior and by analysis of retained species within the pore structure.

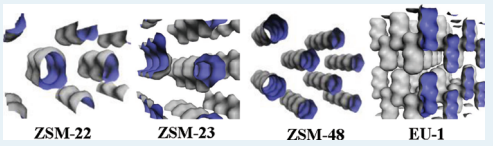

KEYWORDS: MTG, MTO, methanol to gasoline, deactivation, nonaromatic gasoline

1. INTRODUCTION

In contrast to the depleting crude oil reservoirs, the global demand for energy and petrochemical products has been increasing over the years. This calls for both alternative and supplementary sources. Converting low-value carbonaceous feedstocks such as natural gas, coal, or biomass into value-added products is considered as one way of alleviating energy shortage. Methanol is a highly relevant chemical intermediate in this respect, because it may be produced from synthesis gas obtained by gasification of, in principle, any of the feedstocks mentioned above. The methanol-to-hydrocarbons (MTH) reaction, wherein methanol is converted to various hydrocarbons over acidic zeolite catalysts, is thus the final step in such a series of processes. Zeolites are aluminosilicates with strongly acidic Brønsted sites dispersed within a network of pores of near molecular dimension.

Because the MTH reaction occurs mainly within the zeolite crystals, the product selectivity of the reaction depends strongly on the size and dimensionality of the zeolite channel system; that is, product shape selectivity is important. Typically, medium-pore (10-ring) zeolites such as ZSM-5 (three-dimensional channels of size 5.4 × 5.6 and 5.3 × 5.5 Å) display high selectivity for C_{5+} hydrocarbons (aromatics and alkanes), and the process is referred to as methanol-to-gasoline (MTG). On the other hand, small-pore (8-ring) materials such as SAPO-34 (three-dimensional cage structure with window size of 3.8 × 3.8 Å) give high selectivity for C_2 and C_3 hydrocarbons, and the process is referred to as methanol-to-olefins (MTO).[1]

The MTH process has gained industrial attention, and intense industrialization efforts are ongoing. Several alternative processes are commercially available, and several of these rely on ZSM-5 zeolite as a catalyst. These include the Mobil Oil MTG process,[2] the Topsøe integrated gasoline synthesis process,[3] and the Lurgi methanol to propene process.[4] In the latter case, the selectivity is optimized toward propene rather than C_{5+} by tuning the reaction conditions (high temperature and low pressure) and employing a recycle. The Norsk Hydro/UOP MTO process uses SAPO-34 as a catalyst.[5]

Received: October 10, 2011
Revised: November 11, 2011
Published: November 14, 2011

Since the discovery of the MTH reaction in the 1970s,[6] several possible reaction mechanisms have been proposed.[7] The formulation of the hydrocarbon pool mechanism by Dahl and Kolboe[8−10] has led several research groups to a unified view on the reaction mechanism.[11−17] The hydrocarbon pool mechanism postulates that the species trapped or adsorbed within the catalyst pores during the MTH reaction may act as reaction centers to which methanol is continuously added and light alkenes are split off in later reaction steps. Detailed mechanistic investigation of the reaction over ZSM-5 revealed that the reaction proceeds through two distinct pathways, and this notion is known as the dual cycle concept.

In one of these cycles, aromatic species (methylbenzenes) serve as reaction centers, whereas in the other, repeated methylation and cracking of alkenes contribute to product formation. The alkene methylation/cracking pathway is related to the original overall mechanistic proposal by Dessau for the MTH reaction over ZSM-5,[18,19] with an important distinction for the formation of ethene. It has been demonstrated that for ZSM-5, most of the ethene is formed via aromatic reaction centers and that, to a limited extent, ethene is involved in the alkene methylation/cracking pathway. This fundamental insight leads to several possibilities for selectivity control, as it is possible to manipulate the relative contribution from each cycle, thereby adjusting the yield of ethene. Moreover, the identity of the aromatic hydrocarbon pool species is dependent on the zeolite topology.

For the ZSM-5 and H-beta (12-ring; three-dimensional channels of size 6.6 × 6.7 and 5.6 × 5.6 Å), the less substituted methylbenzenes and the fully substituted methylbenzenes were reported to be the active centers, respectively, also influencing the ethene/propene ratio.[13,20,21] Mechanistic studies for the ZSM-22 zeolite (one-dimensional channels of size 4.6 × 5.7 Å) have shown that the aromatics-based hydrocarbon pool reaction mechanism contributes very little to the overall methanol conversion and that the reaction proceeds mainly via the alkene methylation/cracking pathway,[22,23] resulting in a low yield of ethene. In addition, a very high selectivity toward branched C_{5+} hydrocarbons combined with a very low selectivity for aromatics was obtained. This possibility of very nearly extinguishing the aromatics based cycle was ascribed to the narrow one-dimensional 10-ring channels of the material.[22,23]

The observed high selectivity for branched C_{5+} hydrocarbons and the formation of very small amounts of aromatics over ZSM-22 catalyst makes it a very interesting catalyst for the production of environmentally friendly gasoline. Despite that aromatics are octane boosters, there are limits on aromatics in gasoline fuel, and they are considered as environmentally unfriendly.[24] This is due to the fact that these compounds can cause environmental and health problems,[25] and furthermore, high-melting-point aromatics can lead to clogging of the fuel injection system of the engine.[26] Thus, from this perspective, the ideal gasoline consists of aromatic-free, branched alkanes consisting of 5−10 carbon atoms.[24] Interestingly, these requirements can be met by hydrogenating the C_{5+} fraction obtained from the MTH process over ZSM-22 catalyst. From a more fundamental perspective, a ZSM-22-based process might offer flexibility in MTH applications, because the product is intermediate to that formed over SAPO-34 (MTO) and ZSM-5 (MTG).

However, compared with other catalysts and ZSM-5 in particular, the stability of the ZSM-22 toward deactivation is lower.[27,28] Thus, a high-priority issue will be to increase the lifetime of the ZSM-22 catalysts or, alternatively, to find catalyst with similar product selectivities and improved lifetimes. Clearly, other zeolites having 10-ring, 1-dimensional channel systems exist, and one strategy to meet this objective is to synthesize and compare the catalytic performance of such material. Recently, comparative studies of 3-dimensional, 10-ring zeolites have shown that small variations in channel dimensions can lead to significant differences in the stability of the zeolites toward deactivation.[27] Thus, in this contribution, we extend our previous work on ZSM-22[22,29] to investigate the influence of slight variations in channel size and shape of 1-dimensional, 10-ring zeolites on the product distribution; stability is also investigated at various reaction conditions. Four structurally different catalysts (ZSM-22, ZSM-23, ZSM-48, EU-1, see section 3.1) have been synthesized, characterized, and tested as MTH catalysts. To the best of our knowledge, the results presented here constitute the first thorough description of the catalytic performance of ZSM-23, EU-1, and ZSM-48 in the MTH reaction in the regular scientific literature. The results highlight how subtle changes in pore size may dramatically influence product selectivity, thus underscoring the complex mechanisms leading to product shape selectivity in zeolite catalysis. Moreover, two different ZSM-22 catalysts (different crystal size and morphology) are compared to investigate also the effects of changing the catalyst properties within one topology.

2. EXPERIMENTAL SECTION

2.1. Catalyst Synthesis. *2.1.1. ZSM-22.* Commercially available and in-house-synthesized ZSM-22 catalysts, denoted here after as ZSM-22 (C) and ZSM-22 (H), respectively, were studied. The ZSM-22 (C) catalyst having Si/Al = 50 was supplied by Zeolyst International. The ZSM-22 (H) catalyst was synthesized following the synthesis procedure in the literature[22,29,30] with minor modifications. An aqueous solution of potassium hydroxide (2.39 g (Merck) in 10.89 g water), aluminum sulfate (1.06 g (J. T. Baker) in 10.89 g of water) and diaminooctane (6.23 g (Fluka) in 43.6 g of water) were mixed, and Ludox AS-30 solution (28.5 g (Sigma-Aldrich) in 16.14 g of water) was added under vigorous stirring. The resulting gel, with a composition of 8.9 K_2O/1.0 Al_2O_3/90 SiO_2/3 K_2SO_4/27.3 DAO/3588 H_2O, was transferred into a Teflon-lined stainless steel autoclave and crystallized in an oven with an inset that tumbles the autoclave (37 rpm) for 3−4 days at 160 °C. The product was recovered by filtration, washed, dried, and calcined as described in ref 22. The calcined samples were ion-exchanged three times in 1 M NH_4NO_3 solutions for 2 h at 70 °C and again calcined to desorb ammonia as described in ref 22.

2.1.2. EU-1. The preparation of EU-1 in alkaline media was based on a combination of synthesis procedures reported by Shin et al.[31] and Lee et al.[32] using hexamethonium bromide ($HMBr_2$, J&K Scientific) as a structure directing agent (SDA). Colloidal silica (Ludox AS-30, Sigma-Aldrich), aluminum nitrate (98%, Fluka), and sodium hydroxide (Merck) were used as reagents. In a typical synthesis, 0.36 g of aluminum nitrate was mixed with 18.02 g of water and stirred until a clear solution was obtained. A 1.37 g portion of a 50 wt % solution of sodium hydroxide was added to the aluminum nitrate solution and stirred until a homogeneous solution was obtained, followed by addition of 1.55 g of the SDA. After homogenizing the solution, 5.71 g of Ludox AS-30 was added, and the mixture was manually stirred for 5 min. The synthesis mixture with a composition of 30 SiO_2/0.5

dx.doi.org/10.1021/cs200517u |ACS Catal. 2012, 2, 26–37

Al_2O_3/9.0 Na_2O/4.5 $HMBr_2$/1335 H_2O was transferred into 45 mL autoclaves and crystallized in an oven under tumbling for 14 days at 160 °C as described above. The final product was quenched, recovered by centrifugation, and repeatedly washed with distilled water and dried at 60 °C overnight. The organic template was removed by calcining the dried samples at 550 °C in a 50:50 N_2/O_2 mixture for 9 h, including 4 h during which the temperature increased from ambient temperature to 550 °C. The calcined sample was ion-exchanged three times in 1 M NH_4NO_3 solutions for 2 h at 70 °C and again calcined as for the organic template removal.

2.1.3. ZSM-48. ZSM-48 was synthesized with preprepared pentamethonium bromide ($PMBr_2$) as a SDA, as described in the literature.[32] Briefly, 15 g of dibromopentane (DBP, Sigma-Aldrich) was mixed with 31.1 g of 33 wt % trimetylamine (TMA) solution in ethanol (Sigma-Aldrich) and 75 mL of ethanol, giving a relative molar ratio of 2.5:1 of TMA/DBP. The mixture was refluxed overnight, cooled, filtered, and dried at 70 °C. The zeolite was synthesized by mixing 0.22 g of aluminum nitrate (98%, Fluka) with 17.93 g of water and stirred to a clear solution, followed by addition of 0.64 g of a 50 wt % solution of sodium hydroxide and homogenization. To the resulting solution, 1.24 g of the SDA was added, and the mixture was stirred until a homogeneous solution was obtained. Last, 4.96 g of tetraethyl orthosilicate (Sigma-Aldrich) was added, and the mixture was again stirred until all the ethanol was evaporated, typically for 2 h at room temperature before heating the beaker to accelerate the evaporation. The final synthesis mixture with a composition of 30 SiO_2/0.375 Al_2O_3/5.0 Na_2O/4.5 $HMBr_2$/1200 H_2O was transferred into 45 mL autoclaves, and the crystallization was performed in an oven with an inset that tumbles the autoclaves (37 rpm) at 160 °C for 7 days. The final product was quenched, recovered by centrifugation and repeatedly washed with water before being dried overnight. The dried samples were calcined to remove the organic template, ion-exchanged, and calcined again to desorb ammonia as described for EU-1 zeolite, above.

2.1.3. ZSM-23. A commercially available ZSM-23 catalyst having Si/Al = 23 was supplied by Zeolyst International.

2.2. Catalyst Characterization. Crystallinity and purity of the catalysts was determined using X-ray diffraction (XRD). The measurements were performed using a Siemens Bruker D5000 instrument in transmission Debye−Scherrer geometry and Cu $K_{\alpha 1}$ radiation. Scanning electron micrographs (SEM) images revealed the size and shape of the catalyst. FEI Quanta 200 FEG-ESEM equipped with an Everhart−Thornley detector was used for the measurement. BET surface areas of the catalysts were determined using nitrogen physisorption measurements at liquid nitrogen temperature. The samples were outgassed under vacuum for 5 h, 1 h at 80 °C, and 4 h at 300 °C before the measurements. A Belsorp-mini II instrument was used for the measurement. The Si/Al ratio of the materials was calculated using temperature-programmed desorption (TPD), assuming that one ammonia molecule corresponds to one Al substitution.

2.3. Catalytic Tests and Product Analysis. Catalytic tests were carried out in a temperature range between 350 and 500 °C using 50 mg catalyst in a fixed bed reactor (i.d. 10 mm). Before each catalytic test, the protonated catalysts were pressed, gently crushed, and sieved to particle sizes between 250 and 420 μm. The pressed and sieved catalysts were calcined in situ at 550 °C under a flow of pure oxygen for 1 h as described in refs 22 and 29 prior to the feeding of methanol. The in situ calcination is performed to remove species adsorbed during catalyst handling and storage and is important for the reproducibility of the results. Methanol was fed by passing He through a saturation evaporator kept at 20 °C (p_{MeOH} = 130 mbar). Weight hourly space velocities (WHSV) between 2 and 6 g g^{-1} h^{-1} flows were achieved. The reaction products were analyzed as described in detail in the literature.[22] Briefly, the gas phase products were analyzed using a gas chromatograph connected directly to the reactor outlet by a heated transfer line to avoid condensation of heavy products. An Agilent 6890A GC with FID, equipped with a Supelco SPB-5 capillary column (60 m, 0.530 mm i.d., stationary phase thickness 3 μm) was used for the analysis. The temperature of the oven was programmed between 45 and 260 °C with a heating rate of 25 °C min^{-1} (hold time = 5 min at 45 °C and 16 min at 260 °C).

2.4. Analysis of Retained Material. Organic species trapped in the channels or side pockets of the catalysts during the MTH reaction after different times on-stream were analyzed by dissolving 20 mg of the used catalyst in a screw-cap Teflon vial using 15% HF (1 mL).[22] Dichloromethane (1 mL) having hexachloroethane as internal standard was used to extract the organic phase and was analyzed using GC/MS. The aqueous phase was not neutralized prior to extraction. An Agilent 6890N gas chromatograph connected to an Agilent 5793 mass-selective detector equipped with a HP-5MS column (60 m, 0.25 mm i.d., stationary phase thickness 0.25 μm) was used for the analysis. The temperature of the oven was programmed between 50 and 300 °C with a heating rate of 10 °C min^{-1} (hold time = 3 min at 50 °C and 15 min at 300 °C). The compounds were identified by comparing with the mass spectral library of the NIST98 database.

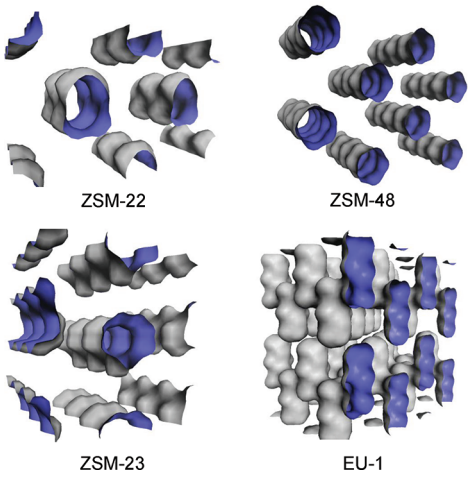

Figure 1. Illustrations of the channel system of ZSM-22 (top left panel), ZSM-48 (top right panel), ZSM-22 (bottom left panel), and EU-1 (bottom right panel) zeolites.

Table 1. Description of the Channel Systems of the Investigated Catalysts

		10-ring channel system		
topology	material	size	shape	side pocket
TON	ZSM-22	5.7 × 4.6 Å	elliptical	none
MTT	ZSM-23	5.2 × 4.5 Å	teardrop	very small
*MRE	ZSM-48	5.6 × 5.3 Å	cylindrical	none
EUO	EU-1	5.4 × 4.1 Å	zig-zag	6.8 × 5.8 × 8.1 Å

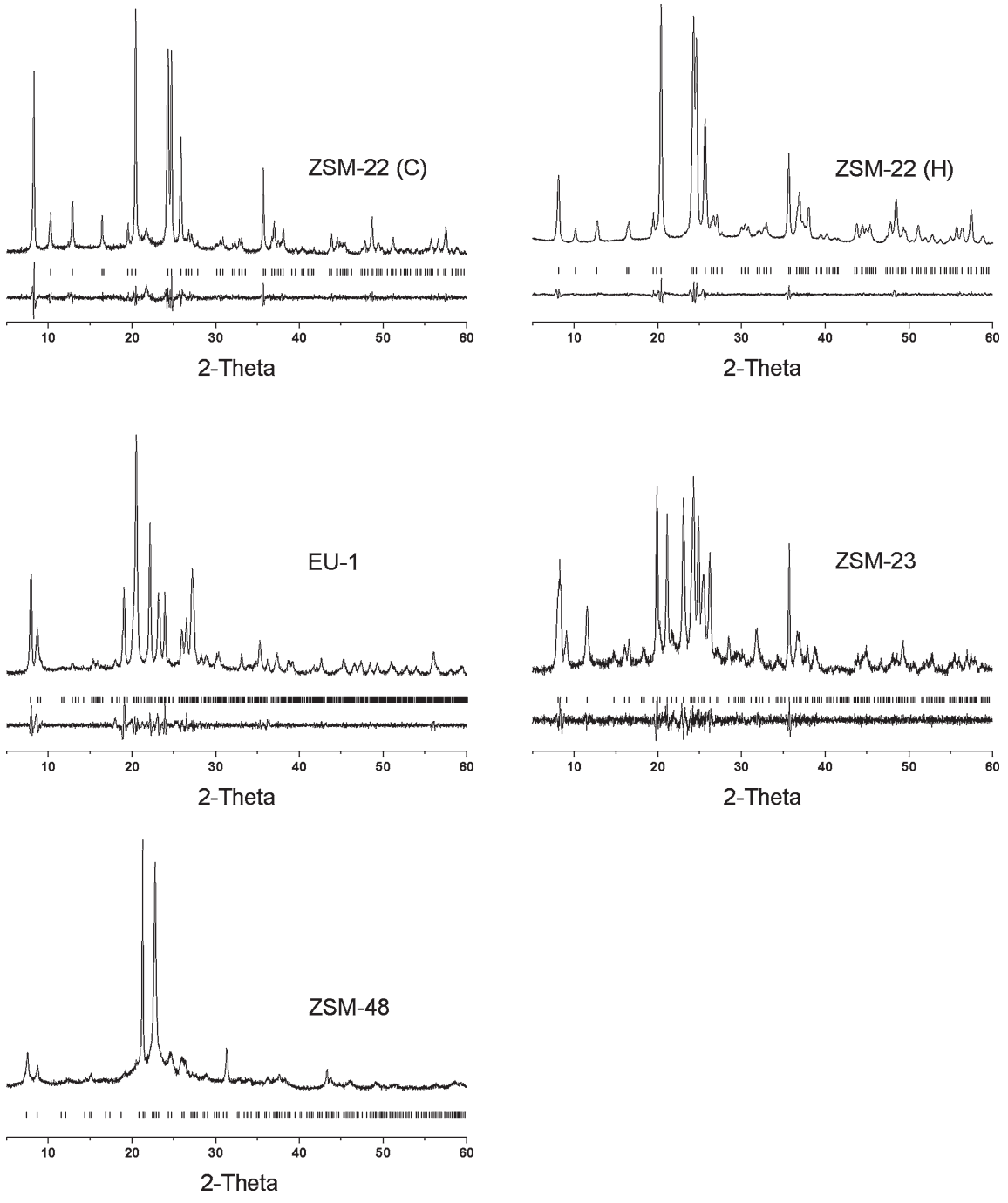

Figure 2. X-ray diffractogram of EU-1, ZSM-22 (C), ZSM-48, ZSM-22 (H), and ZSM-23 catalysts. The bars and the profiles under the diffraction patterns represent theoretically calculated peak positions and differences between experimental and simulated diffraction patterns, respectively.

The total amount of retained material after different times on-stream was determined by temperature-programmed oxidation using a Rheometric Scientific SAT 1500 instrument. The temperature of the oven was programmed between 25 and 650 °C with a heating rate of 5 °C min^{-1} (hold time = 3 h at 650 °C).

3. RESULTS AND DISCUSSIONS

3.1. Description of Catalyst Topologies. The 10-ring channel systems of the materials studied here are illustrated in Figure 1, and key pore dimensions are summarized in Table 1.

As seen from Table 1 and Figure 1, ZSM-48 has nearly symmetrical straight channels with dimensions of 5.3 × 5.6 Å.[33] ZSM-22 has slightly elliptical and slightly zig-zag channels with dimensions of 5.7 × 4.6 Å.[34] ZSM-23 has a teardrop-shaped channel system with dimensions 5.2 × 4.5 Å.[34] The channels of ZSM-23 can be described as having very a small side pocket. EU-1 has channels with dimensions 5.4 × 4.1 Å and 12-ring side pockets.[34] The 12-ring side pockets are 6.8 × 5.8 Å wide and 8.1 Å deep.[35] Thus, the materials studied herein may be viewed as a series of catalysts with very similar one-dimensional pores with perpendicular extensions or side pockets of sizes increasing in the

dx.doi.org/10.1021/cs200517u |*ACS Catal.* 2012, 2, 26–37

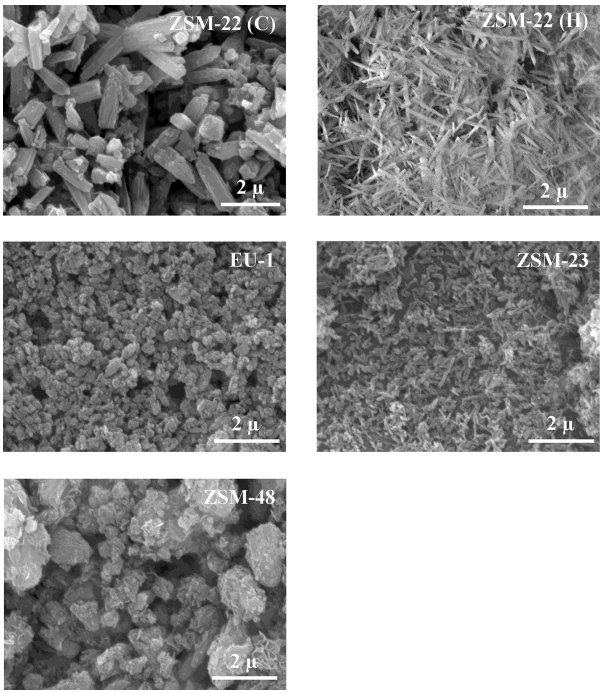

Figure 3. SEM images of ZSM-22 (C) (top left panel), ZSM-23 (top right panel), EU-1 (middle left panel), ZSM-48 (middle right panel), and ZSM-22 (H) (bottom left panel).

order ZSM-48 ≤ ZSM-22 < ZSM-23 < EU-1. Alternatively, the catalysts may be ranked according to the largest single distance/opening giving rise to the series ZSM-23 ≤ ZSM-22 < ZSM-48 < EU-1. It should also be noted that, considering the 10-rings only, EU-1 is the most confined material.

3.2. Catalyst Characterization Results. In this section, the results obtained using powder XRD, SEM, BET, and NH_3-TPD are presented and discussed.

3.2.1. XRD. Figure 2 displays diffractograms for the ZSM-22 (C), ZSM-23, ZSM-48, EU-1, and ZSM-22 (H) catalysts. Calculated peak positions and the differences between experimentally observed diffractograms and those obtained from a Pawley refinement are presented under each diffraction pattern. On the basis of the qualities of the refinements, it may be stated that the materials are crystalline and pure, except from a very small extra peak at 2-θ angle 21.7° for ZSM-22 (C), which corresponds to a dense phase, cristobalite.[36,37] Because ZSM-48 is a disordered structure, a very broad diffraction pattern typical for disordered structures was obtained, and a Pawley refinement was not attempted. However, the diffractogram obtained does match those published elsewhere.[32,38]

3.2.2. SEM. Figure 3 displays SEM images of the ZSM-22 (C), ZSM-23, EU-1, ZSM-48, and ZSM-22 (H) catalysts. One-dimensional zeolites typically display needlelike morphologies,[39−41] and for some phases, it has previously been demonstrated that the channel systems run along the direction of the needles.[40,42] The ZSM-22 (C) and ZSM-22 (H) catalysts do consist of elongated crystals of ∼2 μm in length. However, the ZSM-22 (H) sample displays needle-shaped crystals that are substantially thinner and slightly longer than the ZSM-22 (C) crystals. ZSM-23 catalyst exhibits thin needle-shaped crystals of less than 1 μm in length. The crystals in EU-1 zeolite were very small, less than 0.5 μm and round in shape. We have, however, observed rod-/needle-shaped crystals of less than 1 μm for another batch of EU-1 (not included here). The ZSM-48 sample displayed a different morphology from the usual needle-shaped crystals. Irregular plate and rod-/needlelike (∼2 μm) crystals with no uniform crystal morphology were observed; a similar observation was previously reported.[43] From these results, it seems that needle-/rod-shaped crystals are typical, but not the only possible morphology for 1-dimensional, 10-ring zeolites.

Table 2. Main Characteristics of the Investigated Catalysts

		Si/Al		particle	
material	BET (m^2/g)	gel/supplier	TPD	shape	size (μm)
ZSM-22 (H)	173	45[a]	33	needles	2−3
ZSM-22 (C)	196	50[b]	48	rods	1−2
ZSM-23	115	26[b]	33	needles	<1
ZSM-48	275	40[a]	52	rods	1−2
EU-1	420	30[a]	30	rods	<1

[a] Composition of the synthesis gel. [b] As provided by the supplier.

3.2.3. BET. BET surface area measurements revealed that the ZSM-22 (C), ZSM-23, EU-1, ZSM-48, and ZSM-22 (H) catalysts had BET surface areas of 196, 115, 420, 275, and 173 m^2/g, respectively. Surface areas in this range have been reported for the materials, although the value found for ZSM-23 appears to be in the lower part of the range reported.[44−48]

3.2.4. Ammonia TPD. Temperature-programmed desorption of ammonia from the acid sites of the catalysts was performed to quantitatively measure the density of acid sites. Moreover, the shape of the desorption profile contains information about the distribution of acid strength. The profiles are presented in the Supporting Information. The Si/Al ratios of the materials calculated from the adsorption capacity of ammonia are presented in Table 2.

The values are similar to the Si/Al ratio in the synthesis gel (for ZSM-22 (H), ZSM-48, and EU-1) and those provided by the supplier (for ZSM-22 (C) and ZSM-23). In addition, it should be noted that the densities of acid sites are reasonably similar among the catalysts employed here. It is well-known that the density of acid sites has a profound influence on the activity and lifetime of zeolite catalysts.[49] Inspection of the desorption profiles reveals that the catalysts fall into two groups: First, ZSM-23, ZSM-22 (C), and ZSM-22 (H) catalysts displayed similar desorption profiles, comprising the typical high temperature and low temperature desorption maxima.[50,51] The desorption maximum at high temperature is assigned to desorption of ammonia from strong acid sites. An additional small signal reaching its maximum at ∼230 °C, and partly overlapping with the main peak at ∼420 °C, was observed. This desorption at lower temperature is assigned to desorption ammonia from weak acid sites. Second, ZSM-48 and EU-1 display a single, very broad desorption signal. The very broad ammonia desorption peak reaches its maximum at ∼310 °C for ZSM-48 and at ∼370 °C for EU-1. In principle, it is possible to obtain quantitative information regarding acid site strength by comparing the temperature of maximum desorption. However, such evaluations will be strongly influenced by other parameters, such as crystal size and acid site densities, affecting diffusion and the probability of readsorption.[52] Thus, no such attempt to rank the catalysts according to acid strength based on the NH_3-TPD experiments is performed.

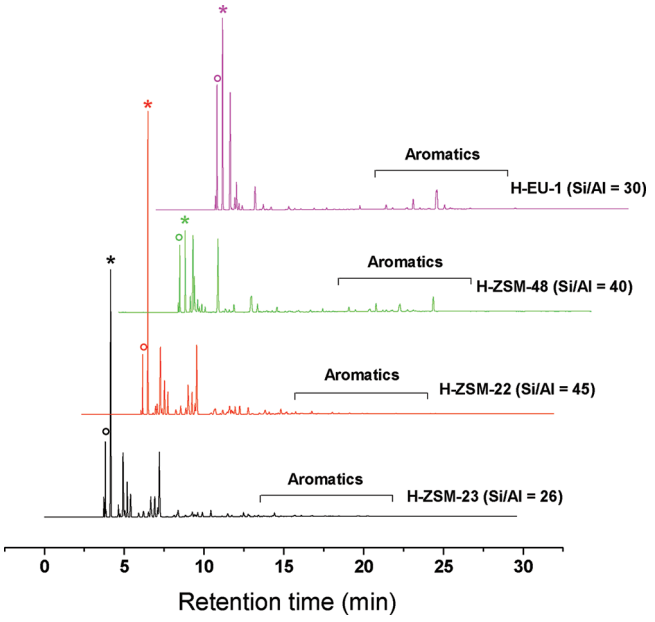

Figure 4. GC-FID chromatograms showing the product distribution in the conversion of methanol to hydrocarbons over ZSM-22 (C) (5.7 × 4.5 Å), ZSM-23 (5.2 × 4.5 Å), EU-1 (5.4 × 4.1 Å), and ZSM-48 (5.6 × 5.3 Å) catalysts after 3 min on-stream. Reaction carried out at WHSV = 2 g g^{-1} h^{-1} and 400 °C. The C_2 and C_3 peaks are indicated using the symbols ° and * on top of the peaks, respectively.

To summarize, from the characterization results, it is shown that the catalysts have particle sizes ranging from <1 to 2−3 μm. Only some of the materials display the expected preference for a needle-shaped morphology. The Si/Al ratios of the catalysts, as determined from NH_3-TPD, are within a limited range of 30−52. XRD revealed that, except from an insignificant amount of a dense phase in ZSM-22, the catalysts are single phase and crystalline. All materials exhibit acceptably high BET surface areas. On the basis of these similarities, it appears reasonable to assign major differences in catalytic performance to differences in topologies (see section 3.3).

3.3. Catalytic Performance in the MTH Reaction. In the following selections, the catalytic performance of the materials (ZSM-22, ZSM-23, ZSM-48, and EU-1) in the MTH reaction is presented. Product distribution of the process over the materials at 400 °C and selectivities for the desired C_{5+} fraction at various reaction temperatures are discussed in detail. Catalytic performance of ZSM-22, ZSM-23, and EU-1 zeolite are investigated at various feed rates (contact times) of methanol, and on the basis of the results, the influence of coke on the MTH reaction selectivity of the materials is presented.

3.3.1. Product Shape Selectivity. Figure 4 displays GC/FID chromatograms of the gas phase effluent of the catalysts obtained during the MTH reaction under identical test conditions, at 400 °C and WHSV = 2 g g^{-1} h^{-1}. The GC-FID analyses were performed after 3 min on-stream. At these conditions, all catalysts gave very nearly full conversion, except ZSM-48 (5.6 × 5.3 Å), for which a conversion of 88% was achieved. Somewhat surprisingly, the product distribution shown for the rod-shaped ZSM-22 (C) (5.7 × 4.5 Å) catalyst is indistinguishable from that previously reported for the needle-shaped ZSM-22 (H) (not shown) catalyst,[22] despite the differences in morphology. The salient feature of the ZSM-22 product spectrum in this context is the near complete absence

Table 3. C_4 Hydrogen Transfer Index (C_4 HTI) and C_2/C_3 Ratio (carbon based) over ZSM-22 (C), ZSM-22 (H), ZSM-23, ZSM-48, and EU-1 Catalysts at Different Conversion Levels Given in Parentheses[a]

catalyst	ZSM-22 (C)	ZSM-22 (H)	ZSM-23	ZSM-48	EU-1
C_4 HTI	0.10	0.07	0.14	0.75	0.86
C_2/C_3 (100%)	0.17	0.15	0.26	0.59 (88%)	0.41
C_2/C_3 (~80%)	0.10	0.08	0.08	0.38	0.32[a]

[a] Interpolated value. [a] Reaction carried out at 400 °C and WHSV = 2 g g^{-1} h^{-1}. C_4 HTI = C_4-alkane/(C_4 alkane + C_4 alkene).

of aromatics in the C_{5+} fraction. Clearly, ZSM-23 (5.2 × 4.5 Å) displays a very similar product shape selectivity compared with the two ZSM-22 catalysts, again without noticeable amounts of aromatic compounds. In agreement with our observation, ZSM-22 and ZSM-23 catalysts were previously reported to give similar selectivity for the conversion of C_4 alkenes to ethene and propene.[53] In addition, these materials show quite similar isomerization selectivity during *n*-octane conversion.[54]

In contrast to these two catalysts, ZSM-48 catalyst displayed a product spectrum comprising substantial amounts of aromatics; several peaks are clearly visible in the aromatic region. This observation might be ascribed to the relatively wider channels of the ZSM-48 catalyst compared with ZSM-22 and ZSM-23. ZSM-48, having channel dimensions very similar to the well-known aromatics yielding ZSM-5 catalyst (5.6 × 5.4 and 5.3 × 5.5 Å), but no channel intersections, clearly must allow the formation and diffusion of aromatics.

Interestingly, the most dominant aromatic compound detected after 3 min on steam over ZSM-48 catalyst was pentamethylbenzene; however, with increasing reaction time, more hexamethylbenzene was observed. The formation of notable amounts of penta- and hexamethylbenzene over ZSM-48 catalyst could be due to pore mouth reactions or flexibility of the zeolite framework and guest species at high temperatures. In contrast, these products are usually insignificant in the ZSM-5 effluent.[22] Surprisingly, EU-1 (5.4 × 4.1 Å) which has channels narrower than the channels of ZSM-22, displayed a product spectrum consisting of aromatic compounds, the dominant aromatic species being tetramethylbenzenes.

Similar to our observation, aromatics have previously been reported in the MTH effluent of EU-1.[55] A plausible explanation for this unexpected product distribution over EU-1 zeolite might be the involvement of the 12-ring side pockets on the outer surface of the crystal during the MTH reaction. These are sufficiently large to allow diffusion of aromatics out of the crystal without passing through the narrow 10-ring channels. A similar phenomenon is well described for the MCM-22 zeolite,[56−59] in which it has been demonstrated that 12-ring surface side pockets contribute to the catalytic behavior, resulting in unexpected selectivity for a medium-pore zeolite. This is probably particle-morphology-dependent, because Bjørgen et al. studied the MTH reaction over MCM-22 and detected very small amounts of aromatics in the gas phase effluent, suggesting that, in that case, the product selectivity was governed mainly by the 10-rings.[60] Hence, we speculate that for EU-1 zeolite, one might obtain aromatic-free hydrocarbons during the MTH reaction if there are no side pockets on the surface of crystals. This might be achieved by tuning the morphology or by passivation of the externals surface. It is important to note that EU-1 has the smallest crystal

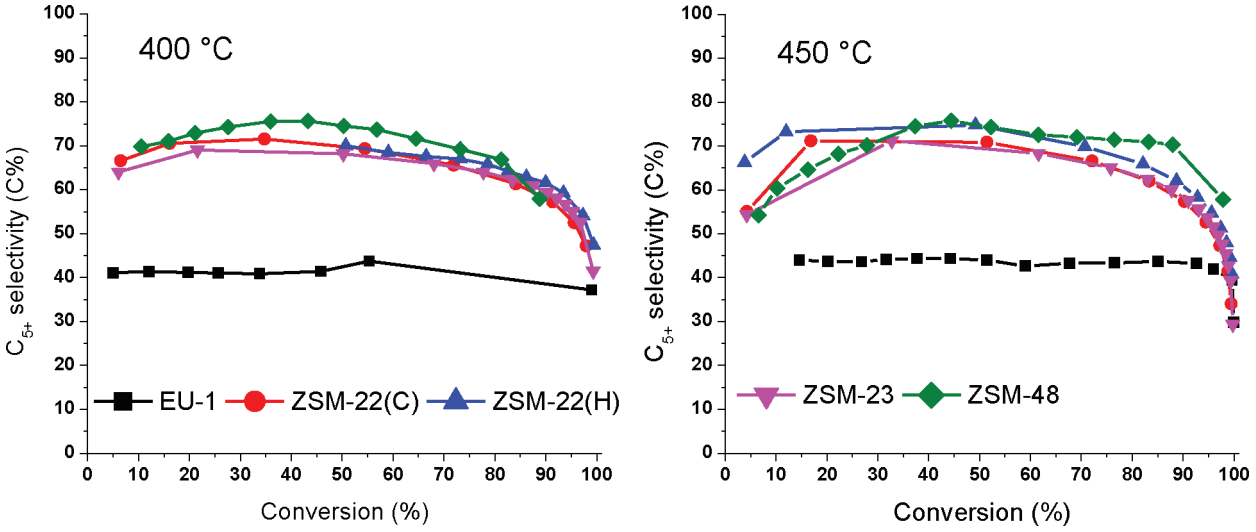

Figure 5. C_{5+} selectivity (carbon-based) as a function of methanol conversion (during gradual deactivation) over EU-1, ZSM-23, ZSM-22 (C), ZSM-48, and ZSM-22 (H) catalysts. Reaction carried out at 400 °C (left panel) and 450 °C (right panel) and WHSV = 2 g g^{-1} h^{-1}. A similar plot showing C_{5+} selectivity versus time on-stream is presented in the Supporting Information.

size and the highest surface area among the materials studied here. Any reactions occurring on the external surface, which in this case might be formation and diffusion of aromatics by involvement of exposed large pores, are likely to be more pronounced over the small crystals of EU-1 than the rest of the materials.

Table 3 displays the C_4 hydrogen transfer index (HTI), which is defined as the selectivity toward butanes divided by the total selectivity toward C_4, and the C_2/C_3 ratio at 400 °C, WHSV = 2 g g^{-1} h^{-1} for the catalysts investigated. The actual conversion levels are also listed in parentheses. The catalysts can be divided into two groups: ZSM-22 and ZSM-23 have low C_4 HTIs and low C_2/C_3 ratios, whereas the opposite is seen for ZSM-48 and EU-1. The observed C_4 HTIs reflect the product distribution presented in Figure 4. Obviously, for EU-1 and ZSM-48, which form hydrogen-poor species in the effluent (aromatics), saturated species must be formed concurrently to match the overall stoichiometry of the process (the H/C ratio should be 2 when not taking coke into account). Thus, the highest C_4 HTIs are found for these two catalysts. Finally, it should be noted that the highest C_2/C_3 ratio was obtained over EU-1 and ZSM-48 catalysts at both full and ∼80% methanol conversion. It is tempting to link this to the possible involvement of the aromatic hydrocarbon pool species for the production of light alkenes (C_2), according to the dual cycle concept outlined in the introduction. However, further mechanistic investigations are needed to verify this hypothesis. In summary, this initial evaluation of the product selectivities found for the four catalyst topologies reveals that the materials fall into two distinct groups: ZSM-22 and ZSM-23 give a C_{5+} fraction virtually free from aromatics, whereas the ZSM-48 and EU-1 product spectra have more in common with the typical aromatic-rich ZSM-5-based MTG product.

3.3.2. Selectivity toward C_{5+} against Reaction Temperature. An overview of the product shape selectivities and a qualitative description of the composition of the gasoline range C_{5+} fraction are given in the preceding section. In this section, a more quantitative examination of the production of the C_{5+} fraction will be discussed. To this end, the product selectivity of the catalysts as a function of methanol conversion levels was monitored at different reaction temperatures. Selected data points for the C_{5+} fractions obtained at 400 and 450 °C are presented in Figure 5. The full data set for the selectivities in the temperatures between 350 and 500 °C is reported in the Supporting Information. A brief discussion for each topology will be given.

Over the ZSM-22 catalysts, depending on the conversion level, selectivities for C_{5+} hydrocarbons between ∼50 and ∼70 C % were observed. At an early stage of the reaction, that is, high methanol conversion, an increase in C_{5+} selectivity with gradual deactivation of the catalyst was observed. This was accompanied by a decrease in the selectivities for the lighter hydrocarbons, mainly the C_3 fraction. This observation can be explained by a decrease in the rate of cracking reaction of the C_{5+} fraction to light alkenes with progressive deactivation of the ZSM-22 catalysts. The selectivity trend observed over ZSM-23 catalyst was very similar to the trend over the ZSM-22 catalysts. C_{5+} selectivity between ∼40 and ∼70 C% was observed. Similar to ZSM-22 catalysts, an increase in the C_{5+} selectivity with gradual deactivation of the catalyst, which is accompanied by a decrease in lighter hydrocarbons selectivities, mainly the C_3 fraction, was observed over ZSM-23.

EU-1 displayed a less conversion-dependent and lower selectivity for C_{5+} hydrocarbons, ranging between ∼35 and 45 C %, which includes ∼15 C % selectivity for aromatics. Concomitantly, higher selectivities for C_3 and C_4 hydrocarbons were observed. A definitive explanation for this observation cannot be formulated on the basis of the current data, but it appears likely that this is related to the particular topology of EU-1 and the relative importance of the narrow 10-ring channels and exposed 12-ring side pockets. Clearly, the 10-ring channels of EU-1 are the narrowest in the series of catalysts and might therefore be expected to contribute little to the overall formation of C_{5+} because of diffusion limitations.

The selectivity toward C_{5+} hydrocarbons appears to be slightly higher for the ZSM-48 catalyst compared with ZSM-22 and ZSM-23. It ranges between ∼55 and ∼75 C %, including 20−40 C % selectivity for aromatics. Despite this promising high

dx.doi.org/10.1021/cs200517u |*ACS Catal.* 2012, 2, 26–37

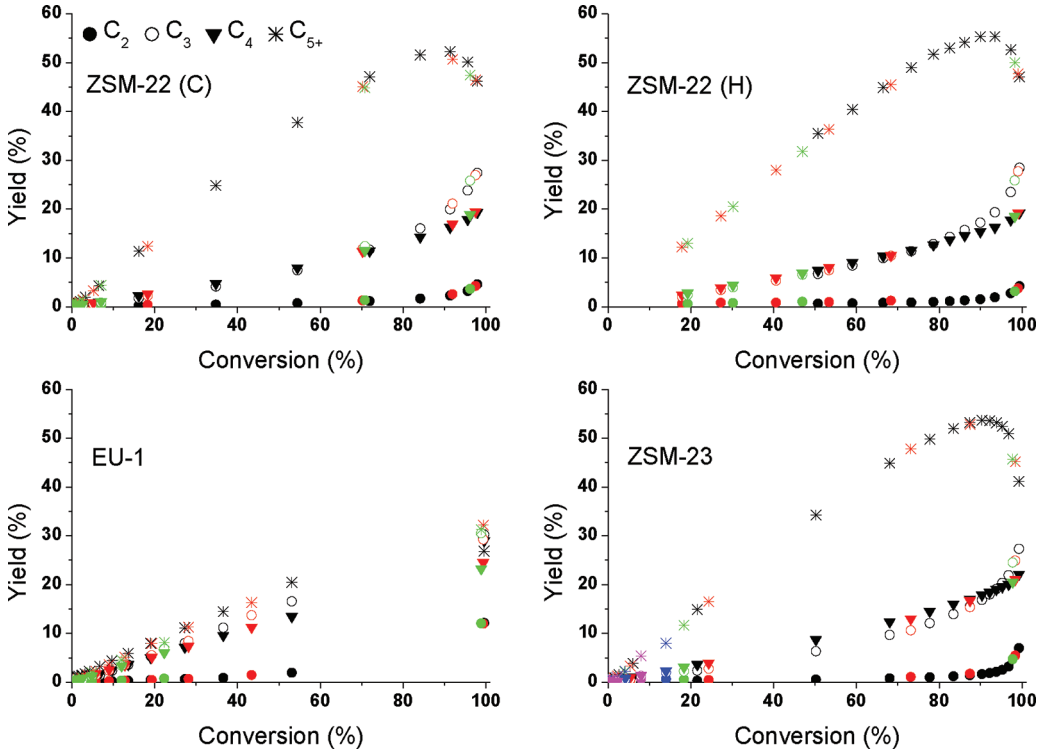

Figure 6. Yield (C %) as a function of methanol conversion (during gradual deactivation) during the MTH reaction over ZSM-22 (C) (top left panel), ZSM-22 (H) (top right panel), ZSM-23 (bottom left panel), and EU-1 (bottom right panel) catalysts. Reactions carried out at 400 °C and WHSV = 2 (black), 3 (red), 4 (green), 5 (blue) and 6 (pink) $g\,g^{-1}\,h^{-1}$. Yield for methane is not included because it is very small. A similar plot showing yield versus time on-stream is presented in the Supporting Information.

selectivity, the formation of considerable amounts of aromatics over ZSM-48 makes the material less competitive toward the production of aromatics-free gasoline. In addition, penta- and hexamethylbenzene are formed to a considerable extent. These compounds are not desirable because of relatively low crystallization temperatures.

Focusing on the initial selectivities, that is, those measured at high methanol conversion, it appears that for the ZSM-22 and ZSM-23 catalysts, for which directly comparable data points are available, increasing the reaction temperature to 450 °C influenced the selectivity toward C_{5+}. Increasing the reaction temperature leads to the formation of higher amounts of lighter hydrocarbons, mainly C_3. In addition, a shift in the internal distribution of the C_{5+} fraction toward lighter compounds was seen at the highest methanol conversion levels (not explicitly shown). The initial selectivity for C_{5+} hydrocarbons over ZSM-22 (H) catalyst was ∼50 C % and dropped to ∼40 C % when the temperature was increased from 400 to 450 °C. Similarly, the initial selectivity for C_{5+} hydrocarbons over ZSM-23 catalyst dropped from ∼40 C % to ∼30 C %. This tendency becomes even clearer when also considering the results at 350 and 500 °C (see the Supporting Information). Clearly, an increase in the reaction temperature leads to a decrease in the selectivity toward C_{5+}. The decrease, which goes along with the increase in the selectivity for lighter fractions while the reaction temperature increases, can be rationalized by both an increased tendency toward cracking of heavier hydrocarbons to lighter fragments at high temperatures[61] and thermodynamic effects. However, the influence of reaction temperature on selectivity should be evaluated keeping also the catalyst lifetime in mind (see below).

For EU-1, the effect of reaction temperature on the initial C_{5+} selectivity was less pronounced. Upon increasing the reaction temperature to 450 °C, EU-1 displayed almost no change in the selectivity for the C_{5+} fraction as the temperature was increased. A stable selectivity of ∼43 C % was obtained, which includes ∼15 C % selectivity for aromatics. Also for the ZSM-48 catalyst, increasing the temperature from 400 to 450 °C appeared to have very little effect on the selectivities: the catalyst displayed high selectivity for the aromatic-rich C_{5+} fraction.

Turning now to the evolution of the selectivities to C_{5+} as a function of conversion/deactivation, it may be stated that for ZSM-22, ZSM-23, and ZSM-48 at a given conversion level less than 100%, the reaction temperature has remarkably little effect on the overall selectivity toward gasoline boiling range hydrocarbons. For EU-1, on the other hand, a slight decrease in the selectivity toward C_{5+} is seen when lowering the reaction temperature.

Clearly, ZSM-22, ZSM-23, and ZSM-48 display a very high selectivity toward C_{5+} hydrocarbons. As a common feature, the selectivity increases with decreasing conversion, that is, with increasing deactivation. Again, the two ZSM-22 catalysts displayed very similar selectivities, despite their different crystal morphologies. In contrast, EU-1 displays a moderate selectivity toward C_{5+}, which appears to be relatively independent of conversion/deactivation.

3.3.4. Influence of Coke Deposition on Selectivity. The selectivity of the methanol-to-hydrocarbon reaction changes with time on-stream. This change might be linked to several parameters, such as formation of coke, which might change the diffusivity of molecules in the zeolite, pore structure, acid site

dx.doi.org/10.1021/cs200517u |*ACS Catal.* 2012, 2, 26–37

density, distribution, or acid site strength etc.[62] Previous studies of the MTH reaction over ZSM-5 catalysts highlighted that the change in product distribution with reaction time may be described as a continuous change in contact time due to a gradual loss of acid sites caused by coking during the reaction.[63] However, it is not obvious that such a relationship should be valid for 1-dimensional zeolites, which one could expect to be very susceptible to pore blocking and changes in diffusion properties. Hence, the influence of coke deposition on the selectivity of ZSM-22, EU-1, and ZSM-23 zeolites was examined. The investigation has been carried out by changing the contact times (WHSV) of the reaction so that a certain level of conversion is reached that corresponds to different degrees of coking.[62,63]

Figure 6 displays yield versus conversion curves during the MTH reaction over the catalysts at 400 °C, and different space velocities are indicated using different colors: WHSV = 2 (black), 3 (red), 4 (green), 5 (blue), and 6 (pink) g g^{-1} h^{-1}. The influence of coke on the selectivity may be described using the ZSM-23 catalyst as a representative example. The initial conversion at WHSV = 6 g g^{-1} h^{-1} over the fresh ZSM-23 catalyst was ∼10%; that is, after feeding, only 0.1 g of methanol per gram of catalyst (clearly, the abrupt drop in initial conversion upon modest increases in feed rate shows that a low feed rate is essential for appreciable methanol conversion over these catalysts, as previously highlighted for ZSM-22[29]), whereas at WHSV = 2 g g^{-1} h^{-1}, 14 g of methanol per gram of catalyst was fed before the conversion dropped to ∼10%. Remarkably, the observed yield at ∼10% conversion over the fresh catalyst at WHSV = 6 g g^{-1} h^{-1} and coked catalyst at WHSV = 2 g g^{-1} h^{-1} were very similar. In the same manner, the amount of coke at all the space velocities (WHSV = 2, 3, 4, and 6 g $g^{-1}h^{-1}$) were different, but similar yields were found at a given conversions. These data strongly suggest that the yield at a certain conversion level is independent of the amount of coke deposited. Thus, the change in selectivity with time on-stream can be regarded as a change in contact time. This also holds when the MTH reaction is carried out over EU-1 and ZSM-22 catalysts. Such behavior has been referred to as nonselective deactivation by Chen et al.,[62] and similar behavior has been reported for ethene oligomerization[62] and MTH reaction over the ZSM-5 catalyst.[63,64] In contrast, selective deactivation was demonstrated for the MTO reaction over SAPO-34, suggesting that, in that case, the coke deposition resulted in changes in the shape selectivity.[62] The conclusion derived from Figure 6, that is, that for a given catalyst sample, the product distribution may be described solely as a function of conversion and appears to be independent of the degree of coking, implies that single event kinetic modeling of the MTH reaction over the catalysts studied here could be achieved by minor modifications of models already developed for ZSM-5.[63]

3.3.5. Catalyst Stability and Total Conversion Capacity. The stability of zeolite catalysts toward deactivation, or lifetime of a catalyst during MTH reaction, is often presented using methanol conversion as a function of reaction time. The stability of a catalyst during the MTH reaction can be described more quantitatively using the total methanol conversion capacity. Total methanol conversion capacity is defined as the total gram amount of methanol converted to hydrocarbons per gram amount of catalyst before complete deactivation.[65,66] It is calculated by integrating the area under the conversion curve and extrapolating to zero conversion.

Table 4 displays total methanol conversion capacities of the catalysts at different reaction temperatures. At 350 °C, the catalysts deactivated very rapidly and converted <1.5 g of methanol per gram of catalyst. Clearly, the optimum temperature for the MTH reaction over the materials is above 350 °C. Increasing the reaction temperature to 400 °C improved the conversion capacities of the catalysts. ZSM-22 (C) and EU-1 catalysts displayed comparable conversion capacities at 400 °C, whereas the ZSM-23 and ZSM-48 catalysts investigated here are substantially more resistant toward deactivation. It should be noted that several ZSM-22 (H) catalysts, synthesized following identical synthesis protocols, were found to have conversion capacities ranging from ∼6 to ∼12 g g^{-1}.[29] This emphasizes that, at this point, it can be misleading to conclude that one catalyst is better than the other on the basis of modest differences. At 450 °C, the ZSM-22 (C) and ZSM-22 (H) catalysts converted ∼9 and ∼11 g g^{-1}, respectively. At this temperature, the conversion capacity of EU-1 was significantly improved, and it reached ∼19 g g^{-1}. ZSM-48 and ZSM-23 catalysts converted ∼14 and ∼16 g g^{-1} at 450 °C. Increasing the temperature to 500 °C resulted in a decrease in the conversion capacity of ZSM-23 catalyst. The ZSM-22 catalysts and EU-1 are less affected when increasing the reaction temperature 500 °C.

Table 4. Total Methanol Conversion, Defined As the Gram Amount of Methanol Converted to Products Per Gram Amount of Catalyst, over ZSM-22 (C), ZSM-23, EU-1, ZSM-48, and ZSM-22 (H) Catalysts

	total conversion capacity at different temperatures			
material	350 °C	400 °C	450 °C	500 °C
ZSM-22 (H)	0.7	6−12[a]	10.5	11.2
ZSM-22 (C)	1.1	6.5	8.5	11.0
ZSM-23	0.3	11.6	16.0	9.3
ZSM-48		15.8	14.3	
EU-1	1.3	5.1	19.2	18.5

[a] Several ZSM-22 (H) batches with different conversion capacities were tested.

The salient feature of Table 4 is that all the materials have comparable stability at their optimum MTH conditions, bearing in mind that the slight differences observed among the topologies are comparable to the differences observed among the different batches of the same topology. In addition, compared with the well-known ZSM-5 catalyst, the catalysts have very low conversion capacities. For ZSM-5, conversion capacities of several hundred g g^{-1} have been reported.[28] For SAPO-34 and H-SSZ-13 (the zeolite analogue of SAPO-34), on the other hand, conversion capacities around 25 g g^{-1} are reported.[67]

It is of primary importance to identify the optimum reaction temperature for each catalyst topology. On the basis of the data in Table 4, it may be confidently stated that ZSM-23 has a lower optimum reaction temperature than ZSM-22 and EU-1. For ZSM-48, the data available are less conclusive. A lower optimum reaction temperature is beneficial, considering both heat requirements and the thermodynamic effect on the selectivity toward C_{5+} mentioned above.

3.3. Composition of Retained Species. The identity and distribution of the compounds retained within the catalyst pores during the MTH reaction was analyzed according to the dissolution/extraction procedure described above. The results are presented as the total ion chromatograms from the GC/MS analyses of the extracts. It should be noted that, on the basis of

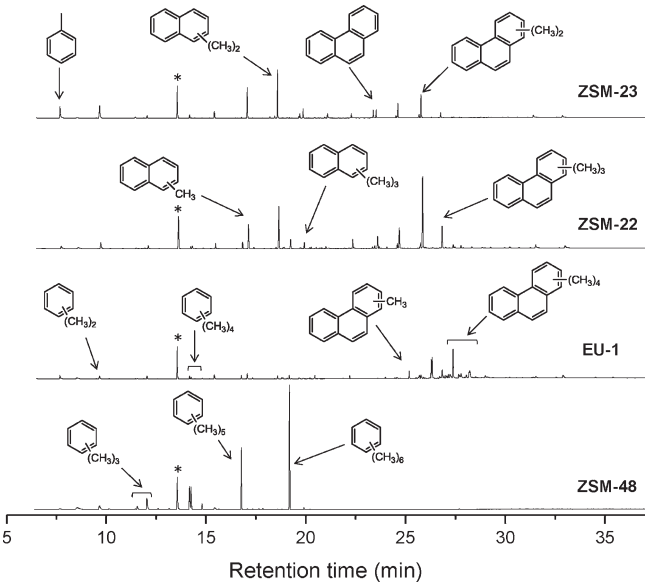

Figure 7. MTH reaction over ZSM-22 (C), ZSM-23, EU-1, and ZSM-48; GC/MS total ion chromatogram of the hydrocarbon extracts of the deactivated catalysts. Reaction carried out at 400 °C and WHSV = 2 g g^{-1} h^{-1}. All the peaks are normalized relative to the standard C_2Cl_6 peak, indicated by the asterisk (*) in the chromatogram.

comparisons with TGA analysis, it appears that for all catalysts, only a part of the coke is soluble in CH_2Cl_2 and amenable to analysis by this technique (see the Supporting Information). The identity of the species trapped during the MTH reaction strongly depends on the zeolite topology. For large-cage zeolites, SAPO-34 and SAPO-18, molecules as large as methyl-substituted pyrenes are trapped and investigated as one cause for deactivation.[68] On the other hand, relatively light species, such as methylbenzenes, are trapped in medium-sized pore zeolite ZSM-5.[69] Depending on the space available, the trapped species can act as active reaction centers (hydrocarbon pool species) and facilitate the methanol conversion[13,69−71] or behave mainly as coke species, which eventually leads to catalyst deactivation.[22] Thus, identification of the trapped species helps to understand the cause of deactivation, which is particularly important for rapidly deactivating catalysts, to identify the MTH reaction centers and gives an indication on the available space for the MTH reaction within the catalyst crystal. Figure 7 displays the GC/MS total ion chromatogram of the hydrocarbon extracts from the fully deactivated catalysts (TOS = ∼20 h) at 400 °C and WHSV = 2 g g^{-1} h^{-1}. The evolution of the retained species with reaction time and temperature is presented in the Supporting Information. Such analyses have previously not been reported for ZSM-23, EU-1, and ZSM-48. A similar discussion has been given for ZSM-22 elsewhere.[29]

Clearly, for ZSM-22 (C) and ZSM-23 catalysts, very similar hydrocarbons were detected as retained species. However, the concentration of relatively heavy species was slightly higher over ZSM-22 than ZSM-23 catalyst, which might be linked to the slightly larger channel dimensions. Even heavier species are trapped in the EU-1 pore structure compared with ZSM-22 and ZSM-23. Moreover, the distribution of retained species is substantially shifted toward heavier compounds. In addition, a substantially larger number of different compounds was detected as trapped species in EU-1 relative to ZSM-22 and ZSM-23, in particular, at lower reaction temperatures and shorter reaction times (see the Supporting Information). Taken together, this strongly suggests the involvement of the more spacious 12-ring side pockets during the reaction. It appears that for the ZSM-23, ZSM-22, and EU-1 catalysts, as the available space increases, relatively more heavy species are trapped. A very different chromatogram was obtained for ZSM-48. Few compounds were detected as trapped species. These are methylbenzenes, with penta- and hexamethylbenzenes as the most dominant species. The retained species over ZSM-48 are, in fact, remarkably similar to those found for ZSM-5 and ZSM-11 catalysts.[27,69] This obvious difference compared with the other 1-dimensional 10-ring structures is rather unexpected, but the current data do not offer any explanation for this particular behavior of the ZSM-48 catalyst. One conclusion may be straightforwardly drawn from the data in Figure 7. All catalysts allow the formation of aromatic species within the pore system; however, only EU-1 and ZSM-48 allow these to diffuse through the channels and desorb into the gas phase. Thus, the particular product spectrum observed for ZSM-22 and ZSM-23 constitutes a typical example of zeolite product shape selectivity.

For ZSM-22, ZSM-23, and EU-1, a reduction in the amount of soluble retained hydrocarbons was observed after a certain time on-stream. However, the total amount of coke as determined by TGA increased with reaction time. A similar effect was seen when increasing the reaction temperature: very little soluble coke could be detected at 450 and 500 °C, even at short reaction times. This strongly suggests a shift in the relative importance of external (insoluble) and internal (soluble) coking as a function of reaction temperature. External coke has been suggested to be the main cause of deactivation in the MTH reaction over ZSM-5.[69,72]

4. CONCLUSIONS

ZSM-22, ZSM-23, EU-1, and ZSM-48 zeolites have been demonstrated to convert methanol to hydrocarbons. The catalysts have comparable stability toward deactivation. Low feed rates and temperature above 350 °C are essential for appreciable conversion over these catalysts. Small differences in the channel system have a notable influence on the product distribution of the MTH reaction over unidirectional 10-ring zeolites. ZSM-22, ZSM-23, and ZSM-48 catalysts give very high selectivity for C_{5+} hydrocarbons; however, an aromatic free C_{5+} fraction is obtained only over ZSM-22 and ZSM-23 pores. This product could meet the requirement for environmentally friendly gasoline after hydrogenation. The side pockets of EU-1 are involved in the MTH reaction and give unexpected catalytic behavior. Aromatic species are formed within the channels of all catalysts, but may apparently diffuse out of only the EU-1 and ZSM-48 catalysts. The change in the selectivities of the MTH reaction over ZSM-22, ZSM-23, and EU-1 zeolites with time on-stream may be described as an effective reduction of contact time because it appears that the development of coke species that might influence the diffusion of molecules does not affect the MTH selectivity over ZSM-22, ZSM-23, and EU-1 catalysts.

■ ASSOCIATED CONTENT

Supporting Information. Temperature-programmed desorption (TPD) profiles, full selectivity data at different reaction temperatures (350−500 °C), C_{5+} selectivity as a function of time on stream plot, yield as a function of time on-stream

plot at different space velocities, GC/MS total ion chromatograms of retained hydrocarbons at different reaction temperatures and different times on stream. This material is available free of charge via the Internet at http://pubs.acs.org.

AUTHOR INFORMATION

Corresponding Author
*Phone: +47 22 85 54 54. Fax: +47 22 85 54 41. E-mail: stian.svelle@kjemi.uio.no.

ACKNOWLEDGMENT

This publication is part of the inGAP Centre of Research-based Innovation, which receives financial support from the Norwegian Research Council under Contract No. 174893. We acknowledge support from Haldor Topsøe A/S.

REFERENCES

(1) Kvisle, S.; Fuglerud, T.; Kolboe, S.; Olsbye, U.; Lillerud, K. P.; Vora, B. V. *Handbook of Heterogeneous Catalysis*, 2nd ed.; Ertl, H., Knözinger, F., Schüth, F., Weitkamp, J., Eds.; Wiley-VCH: Weinheim, 2008; Vol. 6; p 2950.
(2) Cobb, J. In *New Zealand Synfuel: The Story of the World's First Natural Gas to Gasoline Plant*; Connell, G., Ed.; Cobb/Horwood Publications: Auckland, New Zealand, 1995; p 1.
(3) Topp-Jørgensen, J. *Stud. Surf. Sci. Catal.* **1988**, *36*, 293–305.
(4) Koempel, H.; Liebner, W. *Stud. Surf. Sci. Catal.* **2007**, *167*, 261–267.
(5) Chen, J. Q.; Bozzano, A.; Glover, B.; Fuglerud, T.; Kvisle, S. *Catal. Today* **2005**, *106*, 103–107.
(6) Chang, C. D.; J. Silvestri, A. *J. Catal.* **1977**, *47*, 249–259.
(7) Stöcker, M. *Microporous Mesoporous Mater.* **1999**, *29*, 3–48.
(8) Dahl, I. M.; Kolboe, S. *Catal. Lett.* **1993**, *20*, 329–336.
(9) Dahl, I. M.; Kolboe, S. *J. Catal.* **1994**, *149*, 458–464.
(10) Dahl, I. M.; Kolboe, S. *J. Catal.* **1996**, *161*, 304–309.
(11) Arstad, B.; Nicholas, J. B.; Haw, J. F. *J. Am. Chem. Soc.* **2004**, *126*, 2991–3001.
(12) Bjørgen, M.; Olsbye, U.; Svelle, S.; Kolboe, S. *Catal. Lett.* **2004**, *93*, 37–40.
(13) Bjørgen, M.; Olsbye, U.; Petersen, D.; Kolboe, S. *J. Catal.* **2004**, *221*, 1–10.
(14) Sassi, A.; Wildman, M. A.; Ahn, H. J.; Prasad, P.; Nicholas, J. B.; Haw, J. F. *J. Phys. Chem. B* **2002**, *106*, 2294–2303.
(15) Sassi, A.; Wildman, M. A.; Haw, J. F. *J. Phys. Chem. B* **2002**, *106*, 8768–8773.
(16) Arstad, B.; Kolboe, S. *J. Am. Chem. Soc.* **2001**, *123*, 8137–8138.
(17) Haw, J. F.; Song, W. G.; Marcus, D. M.; Nicholas, J. B. *Acc. Chem. Res.* **2003**, *36*, 317–326.
(18) Dessau, R. M. *J. Catal.* **1986**, *99*, 111–116.
(19) Dessau, R. M.; Lapierre, R. B. *J. Catal.* **1982**, *78*, 136–141.
(20) Svelle, S.; Joensen, F.; Nerlov, J.; Olsbye, U.; Lillerud, K. P.; Kolboe, S.; Bjørgen, M. *J. Am. Chem. Soc.* **2006**, *128*, 14770–14771.
(21) Bjørgen, M.; Joensen, F.; Lillerud, K. P.; Olsbye, U.; Svelle, S. *Catal. Today* **2009**, *142*, 90–97.
(22) Teketel, S.; Olsbye, U.; Lillerud, K. P.; Beato, P.; Svelle, S. *Microporous Mesoporous Mater.* **2010**, *136*, 33–41.
(23) Li, J.; Wei, Y.; Qi, Y.; Tian, P.; Li, B.; He, Y.; Chang, F.; Sun, X.; Liu, Z. *Catal. Today* **2011**, *164*, 288–292.
(24) Moulijn, J. A.; Makkee, M.; Diepen, A. V. *Chemical Process Technology*; Jon Wiley and Sons: New York, 2001; p 88.
(25) Kim, B. M.; Park, E. K.; LeeAn, S. Y.; Ha, M.; Kim, E. J.; Kwon, H.; Hang, Y. C.; Jeong, W. C.; Hur, J.; Cheng, H. K.; Yi, J.; Kim, J. H.; Lee, B. E.; Seo, J. H.; Chang, M. H.; Ha, E. H. *J. Prev. Med. Public Health* **2009**, *2*, 96–103.
(26) Olsbye, U.; Svelle, S.; Bjørgen, M.; Beato, P.; Janssens, T. V. W.; Joensen, F.; Bordiga, S.; Lillerud, K. P. *Angew. Chem., Int. Ed.* **2011**, Accepted.
(27) Bleken, F.; Skistad, W.; Barbera, K.; Kustova, M.; Bordiga, S.; Beato, P.; Lillerud, K. P.; Svelle, S.; Olsbye, U. *Phys. Chem. Chem. Phys.* **2011**, *13*, 2539–2549.
(28) Bjørgen, M.; Joensen, F.; Holm, M. S.; Olsbye, U.; Lillerud, K. P.; Svelle, S. *Appl. Catal., A* **2008**, *345*, 43–50.
(29) Teketel, S.; Svelle, S.; Lillerud, K. P.; Olsbye, U. *ChemCatChem* **2009**, *1*, 78–81.
(30) Masih, D.; Kobayashi, T.; Baba, T. *Chem. Commun.* **2007**, 3303–3305.
(31) Shin, J.; Hong, S. B. *Microporous Mesoporous Mater.* **2009**, *124*, 227–231.
(32) Lee, S. H.; Shin, C. H.; Yang, D. K.; Ahn, S. D.; Nam, I. S.; Hong, S. B. *Microporous Mesoporous Mater.* **2004**, *68*, 97–104.
(33) Schlenker, J. L.; Rohrbaugh, W. J.; Chu, P.; Valyocsik, E. W.; Kokotailo, G. T. *Zeolites* **1985**, *5*, 355–358.
(34) Meier, W. M.; Olson, D. H.; Baerlocher, C. *Atlas of Zeolite Structure Types*, 5th ed.; Elsevier: Amsterdam, 2001.
(35) Briscoe, N. A.; Johnson, D. W.; Shannon, M. D.; Kokotailo, G. T.; Mc Cusker, L. B. *Zeolites* **1988**, *8*, 74–76.
(36) Highcock, R. M.; Smith, G. W.; Wood, D. *Acta Crystallogr., Sect. C: Cryst. Struct. Commun.* **1985**, *41*, 1391–1394.
(37) Kokotailo, G. T.; Schlenker, J. L.; Dwyer, F. G.; Valyocsik, E. W. *Zeolites* **1985**, *5*, 349–351.
(38) Li, R. F.; Fan, W. B.; Ma, J. H.; Fan, B. B.; Cao, J. H. *Zeolites* **1995**, *15*, 73–76.
(39) Fan, W. B.; Li, R. F.; Fan, B. B.; Ma, J. H.; Cao, J. H. *Appl. Catal., A* **1996**, *143*, 299–308.
(40) Mõller, K; Bein, T. *Microporous Mesoporous Mater.* **2011**, *143*, 253–262.
(41) Verboekend, D.; Chabaneix, A. M.; Thomas, K.; Gilson, J. P.; Pérez Ramírez, J. *CrystEngComm* **2011**, *13*, 3408–3416.
(42) Hogan, P. J.; Whittam, T. V.; Birtill, J. J.; Stewart, A. *Zeolites* **1984**, *4*, 275–279.
(43) Ferdov, S.; Lin, Z.; Sá Ferreira, R. A. *Chem. Lett.* **2008**, *37*, 100–101.
(44) Li, J.; Qi, Y.; Liu, Z.; Liu, G.; Zhang, D. *Catal. Lett.* **2008**, *121*, 303–310.
(45) Hayasaka, K.; Liang, D.; Huybrechts, W.; De Waele, B. R.; Houthoofd, K. J.; Eloy, P.; Gaigneaux, E. M.; van Tendeloo, G.; Thybaut, J. W.; Marin, G. B.; Denayer, J. F. M.; Baron, G. V.; Jacobs, P. A.; Kirschhock, C. E. A.; Martens, J. A. *Chem.—Eur. J.* **2007**, *13*, 10070–10077.
(46) Huybrechts, W.; Vanbutsele, G.; Houthoofd, K. J.; Bertinchamps, F.; Narasimhan, C. S. L.; Gaigneaux, E. M.; Thybaut, J. W.; Marin, G. B.; Denayer, J. F. M.; Baron, G. V.; Jacobs, P. A.; Martens, J. A. *Catal. Lett.* **2005**, *100*, 235–242.
(47) Xu, Q.; Gong, Y.; Xu, W.; Xu, J.; Deng, F.; Dou, T. *J. Colloid Interface Sci.* **2011**, *358*, 252–260.
(48) Zhao, G. L.; Teng, J. W.; Zhang, Y. H.; Xie, Z. K.; Yue, Y. H.; Chen, Q. L.; Tang, Y. *Appl. Catal., A* **2006**, *299*, 167–174.
(49) Kim, J.; Choi, M.; Ryoo, R. *J. Catal.* **2010**, *269*, 219–228.
(50) Katada, N.; Igi, H.; Kim, J. H.; Niwa, M. *J. Phys. Chem. B* **1997**, *101*, 5969–5977.
(51) Rodriguez-Gonzalez, L.; Hermes, F.; Bertmer, M.; Rodriguez-Castellon, E.; Jimenez-Lopez, A.; Simon, U. *Appl. Catal., A* **2007**, *328*, 174–182.
(52) Rodríguez-González, L.; Simon, U. *Meas. Sci. Technol.* **2010**, *21*, 1–7.
(53) Zhu, X.; Liu, S.; Song, Y.; Xu, L. *Appl. Catal., A* **2005**, *288*, 134–142.
(54) Yunfeng, H.; Xiangsheng, W.; Xinwen, G.; Silue, L.; Sheng, H.; Haibo, S.; Liang, B. *Catal. Lett.* **2005**, *100*, 59–65.
(55) Schulz, H. *Catal. Today* **2010**, *154*, 183–194.
(56) Souverijns, W.; Verrelst, W.; Vanbutsele, G.; Martens, J. A.; Jacobs, P. A. *J. Chem. Soc., Chem. Commun.* **1994**, 1671–1672.

(57) Lawton, S. L.; Leonowicz, M. E.; Partridge, R. D.; Chu, P.; Rubin, M. K. *Microporous Mesoporous Mater.* **1998**, *23*, 109–117.
(58) Ravishankar, R.; Bhattacharya, D.; Jacob, N. E.; Sivasanker, S. *Microporous Mater.* **1995**, *4*, 83–93.
(59) Inagaki, S.; Kamino, K.; Hoshino, M.; Kikuchi, E.; Matsukata, M. *Bull. Chem. Soc. Jpn.* **2004**, *77*, 1249–1254.
(60) Bjørgen, M.; Akyalcin, S.; Olsbye, U.; Benard, S.; Kolboe, S.; Svelle, S. *J. Catal.* **2010**, *275*, 170–180.
(61) Abbot, J.; Wojciechowski, B. W. *Can. J. Chem. Eng.* **1985**, *63*, 451–461.
(62) Chen, D.; Rebo, H. P.; Moljord, K.; Holmen, A. *Ind. Eng. Chem. Res.* **1997**, *36*, 3473–3479.
(63) Janssens, T. V. W. *J. Catal.* **2009**, *264*, 130–137.
(64) Bleken, F.; Janssens, T. V. W.; Olsbye, U. Manuscript in preparation, 2011.
(65) Mikkelsen, Ø.; Kolboe, S. *Microporous Mesoporous Mater.* **1999**, *29*, 173–184.
(66) Bjørgen, M.; Kolboe, S. *Appl. Catal., A* **2002**, *225*, 285–290.
(67) Bleken, F.; Bjørgen, M.; Palumbo, L.; Bordiga, S.; Svelle, S.; Lillerud, K. P.; Olsbye, U. *Top. Catal.* **2009**, *52*, 218–228.
(68) Marcus, D. M.; Song, W. G.; Ng, L. L.; Haw, J. F. *Langmuir* **2002**, *18*, 8386–8391.
(69) Bjørgen, M.; Svelle, S.; Joensen, F.; Nerlov, J.; Kolboe, S.; Bonino, F.; Palumbo, L.; Bordiga, S.; Olsbye, U. *J. Catal.* **2007**, *249*, 195–207.
(70) Hereijgers, B. P. C; Bleken, F.; Nilsen, M. H.; Svelle, S.; Lillerud, K. P.; Bjørgen, M.; Weckhuysen, B. M.; Olsbye, U. *J. Catal.* **2009**, *264*, 77–87.
(71) Svelle, S.; Joensen, F.; Nerlov, J.; Olsbye, U.; Lillerud, K. P.; Kolboe, S.; Bjørgen, M. *J. Am. Chem. Soc.* **2006**, *128*, 14770–14771.
(72) Choi, M.; Na, K.; Kim, J.; Sakamoto, Y.; Terasaki, O.; Ryoo, R. *Nature* **2009**, *461*, 246–249.